AGU PUBLICATIONS

JGR

Journal of Geophysical Research: Oceans

RESEARCH ARTICLE

10.1002/2014JC010481

**Key Points:**

- Tidal characteristics of the sound consistent with a barotropic standing wave
- Subtidal velocity fluctuations were vertical sheared and primarily driven by wind forcing
- Mean along-sound circulation had laterally sheared flow indicative of Coriolis forcing

**Correspondence to:**
B. Dzwonkowski,
briandz@disl.org

**Citation:**
Dzwonkowski, B., N. R. Pettigrew, and S. R. Knapp (2015), Spatial and temporal variability of the velocity and hydrographic structure in a weakly stratified system, Broad Sound, Casco Bay, Maine, *J. Geophys. Res. Oceans*, *120*, doi:10.1002/2014JC010481.

Received 30 SEP 2014
Accepted 2 JUN 2015
Accepted article online 5 JUN 2015



# Spatial and temporal variability of the velocity and hydrographic structure in a weakly stratified system, Broad Sound, Casco Bay, Maine

**Brian Dzwonkowski[1], Neal R. Pettigrew[2], and Stacy R. Knapp[2]**

[1]Dauphin Island Sea Lab, University of South Alabama, Dauphin Island, Alabama, USA, [2]School of Marine Sciences, University of Maine, Orono, Maine, USA

**Abstract** The velocity and hydrographic structure across Broad Sound, a north-south orientated subsystem of Casco Bay, ME that lacks continuous coastal boundaries, were characterized using velocity observations from two moorings in late summer/fall of 2013 and velocity and density observations from a repeat-transect ship survey conducted over a tidal cycle during the same period. At tidal time scales, the system is dominated by a barotropic semidiurnal standing wave with a west to east decrease in tidal amplitude and relatively minimal phase change across the majority of the transect. The stratification (vertical differences of 0.5–1.0 kg m$^{-3}$) was generally laterally uniform and stronger during the flood phase which is hypothesized to result from stronger offshore stratification. The mean circulation had strong lateral shear with inflow over the deepest point in the bathymetric cross section and eastern slope and outflow over the western slope. There was also vertical shearing of the horizontal velocities with stronger northward (or northward trending) velocities at depth. The depth-averaged subtidal fluctuations were relatively small (~2–3 cm s$^{-1}$) and uncorrelated between mooring sites suggesting the vertically uniform current response associated with remote wind forcing is of limited importance. On the other hand, the depth-dependent velocity fluctuations at the subtidal time scale were, in large part (~36–72%), driven by wind forcing. The net flux ratio, a means of quantifying the relative importance of the vertical and lateral shear in the flow field, was typically ~0.44 indicating the structure of the local wind response favored vertically sheared flow.

## 1. Introduction

Many coastal/estuarine systems are characterized by having series of channels separating an irregular network of islands. The complex geometry as well as the temporal and spatial variability in forcing functions of these systems presents a challenge to understanding the driving dynamics and resulting circulation in these regions. With regard to system geometry, there have been many studies that have shown cross-sectional bathymetry can dramatically change the lateral structure of along-channel flow. For example, *Wong* [1994] analytically demonstrated both density-driven and wind-driven circulation changes from a vertically sheared exchange flow in a flat bottom system to a laterally sheared flow in a triangular shaped system. This sensitivity to bottom morphology is expected to be a major flow constraint in estuarine systems with complex three-dimensional morphologies. In addition, the bathymetric constraints of an estuarine system can result in locally varying forcing conditions. For example, island systems can differentially distribute fresh water discharge (e.g., Penobscot Bay, Maine) [*Xue et al*., 2000], leading to variability in density gradients (a primary forcing function) within a system's outflow pathways. Similarly, channel orientation can affect the role of different forcing mechanisms, leading to variability in circulation, and the resulting material transport and salt fluxes. *Chawla et al*. [2008] found the circulation dynamics in the north and south channels in the Columbia River estuary varied due, in part, to differences in exposure to river forcing. In Mobile Bay, a system with two sources of exchange, *Kim and Park* [2012] found the salt balance required net inflow through one connection and net outflow through the other. Furthermore, there was significant variability about the mean conditions for which the relative contributions between the two connections depended on the type of forcing (wind versus discharge) and direction of the forcing, in the case of wind.

Casco Bay, formed by glacial erosion and postglacial sea-level rise, has a rugged bottom topography and complicated island system, typical of many higher latitude coastal regions (Figure 1a). This complex network

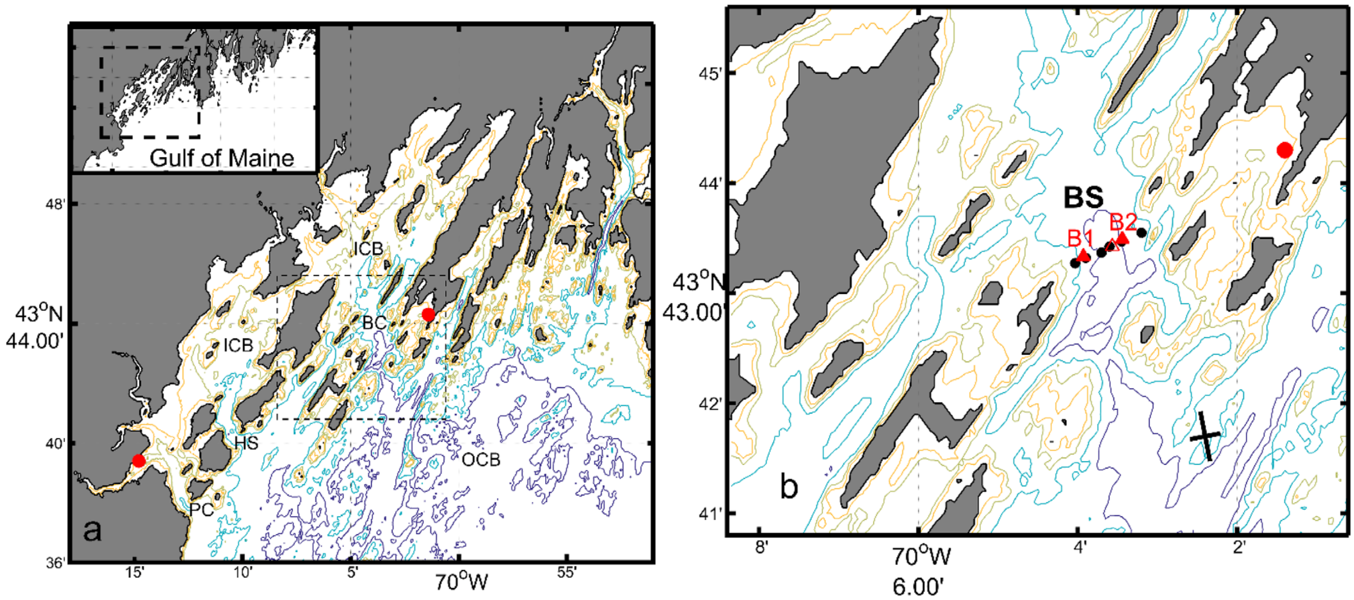


**Figure 1.** (a) A map showing Casco Bay (CB) with its associated bathymetry (black contours are islands and color contours are the 5 m (orange), 10 m (green), 20 m (light blue), and 35 m (blue) isobaths). The NOAA CO-OPS Portland water level station as well as the South Harpswell NOAA CO-OPS tidal prediction station as also shown (red circle). The Portland station is the southwestern location. Inner and Outer Casco Bay, ICB, and OCB, respectively, are labeled as well. The inset shows Casco Bay in the context of the greater Gulf of Maine coastal region. (b) A map showing Broad Sound (BS) and some of the surrounding waterways. The mooring locations are indicated with (red triangle) where the open triangle represents the location of site B2 during Period 1. The ADCP/CTD ship survey stations are shown as (black circle) and are referred to as stations 1–6 going west to east (not labeled). The bathymetry contours and water level station representations are the same as in Figure 1a. Orientation of the velocity observations at the moorings in Broad Sound is indicated by the black cross in the southeast corner with the longer line denoting the along-sound direction as determined by the orientation of the tidal currents (Figure 4).

of channels, ledges, and shoals constrains flow between inner and outer Casco Bay as well as influences exchange between the individual subsystems within the Bay. Casco Bay is a semidiurnal system with a meso-tidal range (~2.0–3.0 m), which has both shallow and deep exchange channels (~0–50 m) that are relatively narrow (~0.5–3.0 km), which can have irregular bathymetric contours as well as moderate curvature. While the bay itself is relatively large, approximately 18 km in length and 32 km in width, it is thought to be separated into two regions (upper and lower Casco Bay) with minimal connectivity [*Sinnett*, 2012]. There are three deep connections to the shelf, Portland Channel and Hussey Sound in the south and Broad Sound in the north, which is the focus of this study (Figure 1). Connecting the upper portion of inner Casco Bay with Outer Casco bay, Broad Sound is a physically short (~3 km), narrow (~2–3 km) passageway that is also exposed to lateral flow due the discontinuous boundaries that consist of a relatively open arrangement of islands and channels. This lack of continuous coastline is in stark contrast to standard idealized estuarine geometries.

Casco Bay presents an additional feature in that it can receive freshwater from both inside and outside the system. Previous hydrographic analysis on the shelf, as well as river flow measurements, show freshwater discharge is dominated by Kennebec-Androscoggin discharge (mean annual discharge rate of 420 $m^3\ s^{-1}$), which occurs approximately ~20 km east of Broad Sound and typically peaks in April (~1000–4000 $m^3\ s^{-1}$), with the resulting buoyancy influx expanding over the shelf and into outer Casco Bay during the spring and summer months [*Janzen et al*., 2005; *Xue and Du*, 2010]. The sources of river discharge in Casco Bay are quite small in comparison to the Kennebec-Androscoggin, with Presumpscot River and Royal River having a combined mean annual rate of less than 40 $m^3\ s^{-1}$ [*Sinnett*, 2012]. Furthermore, the complex channel structure around Broad Sound provides opportunities for buoyancy input from a range of directions, which is different from traditional estuarine systems (i.e., freshwater source at the river head and saline source at the mouth), but is typical of this class of estuary/bay. There is significant seasonality in the freshwater discharge, with peak levels occurring in late winter and early spring and minimum levels occurring in late summer and autumn.

Within estuaries of complex bathymetries where forcing conditions vary locally, the circulation characteristics and dynamics of individual subsystems have the potential to experience significant temporal and spatial variations. Consequently, the relative effect of different forcing functions on the circulation in any given part of a complex system can be difficult to predict. As such, the overall objective of this study is to characterize the spatial and temporal variability in the circulation of a sound in a multichannel system as well as examine the physical processes driving the observed variability in a weakly stratified, meso-tidal system. To this effect, observations from an experiment during late summer/early fall of 2013 in Broad Sound, a deep connection linking upper Casco Bay to outer Casco Bay, are used to better understand circulation in these types of regions. An additional goal of this study is to provide an overview of the spatial and temporal characteristics of the circulation across Broad Sound, as there is only a very limited understanding of the general circulation in Casco Bay.

## 2. Observations and Methods

### 2.1. Observation Sources

During the late summer/early fall (15 August to 16 November) of 2013, two moorings were deployed in Broad Sound to measure water column velocity and metrological measurements (Figure 1, sites B1 and B2). Velocity observations were collected at each mooring with an Aanderaa current meter at 2 m depth and a downward looking RD Instruments 600 kHz ADCP below the current meter to collect velocity measurements through the remainder of the water column. The current meters were programmed to collect velocity measurements every 30 min with 2 min averages and ADCPs were programmed to collect velocity measurements every 30 min with 8 min averages with 0.5 m vertical bins (i.e., ADCP collected measurements at a vertical interval of 0.5 m). The wind observations were collected every 10 min with an 8 min average and subsampled to every 30 min. The wind speed and direction were measured at a height of 4 m with an R.M. Young instrument at site B1 and a Gill sonic anemometer at site B2. There was little difference between the wind measurements. Wind observations from site B1 are used throughout the study as measurements from site B2 did not record until 17 September. Initially, the two moorings were deployed on the western slope and deepest point in the bathymetric cross section of Broad Sound (Figure 1 near stations 2 and 4) at depths of approximately 29 and 45 m, respectively. On 9 September 2013, local fishermen moved mooring B2. The mooring was repositioned to the east of the deepest point in the bathymetric cross section at the request of the fishermen. On 17 September 2013, local fishermen again moved the mooring further onto the eastern slope in approximately 31 m of water (near station 5), where the mooring was left for the remainder of the study period. As such, the observations are divided into three time periods: Period 1 (15 August to 9 September), Period 2 (10 September to 16 September), and Period 3 (17 September to 16 November). This study focuses on Period 3 due to the notably longer duration. However, aspects of site B2 during Period 1 are discussed to provide information on the velocity structure of the deepest point in the bathymetric cross section.

A ship survey was also conducted on 21 September 2013 along a transect across the width of Broad Sound (Figure 1) in which velocity and hydrographic observations were obtained from C-BOLD, a shallow-draft 12.5 m research vessel. Velocity observations were collected with a RD Instruments 600 kHz Workhorse Sentinel ADCP mounted to the side of the vessel, and the hydrographic observations were collected using a SeaBird CTD (SBE 25*plus* Sealogger). The transect consisted of six stations approximated 300 m apart for which velocity measurements were collected while a CTD cast was being conducted. The velocity measurements at the stations were collected using WinRiver II software with GPS positioning and bottom tracking to remove the motion of the vessel. Using 0.5 m vertical resolution, observations were made for approximately 2.0–4.0 min at $\sim$2 Hz with ensemble measurements calculated every eight pings. These ensembles were further averaged for the total sampling period to produce a station measurement. The survey station sampling at stations 2 and 5 avoided times when the mooring instruments were sampling in order to avoid inference issues. At each station, the CTD was soaked for $\sim$1 min at a depth of $\sim$2 m, and then, to capture the near-surface density structure, raised to just below the surface before starting the downcast. This typically provided measurements as shallow as $\sim$1 m. The transect was repeated 14 times (approximately 45 min repeat time) over a tidal cycle so subtidal signals could be obtained.

Additional hourly water level measurements from a NOAA CO-OPS station (#8418150) at Portland were obtained over the study period. While this site is on the opposite end of Casco Bay, a comparison with the local NOAA model tidal prediction for South Harpswell, Potts Harbor (#8417647), the closest tidal prediction site to Broad Sound, are extremely similar. High and low tide predictions are only different by a few minutes between these two sites (not shown). Thus, the water level signal at the Portland station is assumed to be representative of Broad Sound. Bathymetry for the study region was provided by the U.S. Coastal Relief Model which has a resolution of 3 arc sec (NOAA National Geophysical Data Center, http://www.ngdc.noaa.gov/mgg/coastal/crm.html).

### 2.2. Observation Processing and Analysis

The current and wind time series from site B2 were generally continuous; however, the velocity measurements from site B1 had a drifting time step which led to periodic resets in which short measurement gaps occurred (maximum gap length of 6.5 h and totaling to less than 4% of the time series length) and the sampling time shifted by a few minutes. This issue was addressed by interpolating the measurements to the same 0.5 h time step as site B2. The relatively short gaps in the time series were filled by using a tidal fit and a low frequency trend from the available observations. The tidal fit was obtained using harmonic analysis with the T_Tide software package (discussed below) and the low frequency trend was determined by tidally averaging the velocity over 25 h on each side of a gap from which a trend between the two tidal averages was generated using linear interpolation. In addition, several near-bottom measurement bins were excluded from the current velocity analysis to avoid side-lobe contamination by assuming that a distance of approximately 10% of the water depth is lost as a result of these effects. The wind velocity was adjusted to be at a measurement height of 10 m assuming a logarithmic profile [*Large and Pond*, 1981].

A number of analysis procedures were applied to the observations in order to better identify and understand system characteristics. Depth-averaged currents were obtained following *Shearman and Lentz* [2003]. On account of the tidal dominance in the system (discussed in section 3), the along and across-sound orientation were determined using the major and minor axes of the principal components of the depth-averaged instantaneous measurements. This orientation was very similar at both sites and an angle of 349°/169° was used as the along-sound axis with positive (negative) values indicating flow into (out of) Broad Sound. Positive (negative) across-sound velocities are approximately eastward (westward). The principal axes of the subtidal flow were typically small ($<3$ cm s$^{-1}$) and had orientations that were less well defined than the tidal currents with major/minor axis ratios of $\sim$0.4–0.6. The principal axes at site B1 were generally similar throughout the water column and consistent with the tidal ellipse orientations, while site B2 was more variable. This is likely due to the fact that the sound cross section does not follow a line directly joining nearby islands, but rather crosses a bathymetric depression that is a major deep water connection to inner Casco Bay. Consequently, the conceptual framework of a "channel" in the typical sense (i.e., long, uniformly straight system) will not directly translate to this system and so the terms along and across-sound will be used to describe the axial and lateral directions, respectively.

Mean and standard error analysis, following *Lentz* [2008], was used to quantify the uncertainty in the time series means. The along and across-sound uncertainty is typically less than 1.5 cm s$^{-1}$ using a 4.5 day decorrelation time scale to determine the effective degrees of freedom. This is a conservative estimate for most depths as the integral time scale [*Emery and Thomson*, 2004] was typically less than 4.5 days throughout the water column. The near-surface velocity bins had slightly higher standard error values than near-bottom velocity bins. The instantaneous time series of current velocity, wind velocity, and water level were separated into high and low-pass signals using a 40 h low-pass Lanczos filter, where the high-pass signal is considered to be the tidal signal in the case of the currents and water level (i.e., $u_I = u_{lp} + u_{hp} = u_{lp} + u_{tidal}$; where u is the velocity, the subscripts I, lp, and hp refer to the instantaneous, low-pass, and high-pass components of the velocity, respectively). After this separation, additional analyses were applied to these individual time series. This separation follows the methods of *Wong and Moses-Hall* [1998] and allows any nonlinear interactions between tidal and subtidal motions on the intratidal variability to be retained in the tidal signal (i.e., high-pass filtered measurements). For the water level, the NOAA tidal prediction at Portland were used to remove the tides in the water level measurements prior to low-pass filtering the measurements. The NOAA tidal prediction captures greater than 99% of the variance of the high-pass signal; however, for consistency with the velocity measurements, the high-pass signal is shown rather than the tidal prediction as there is little difference between the two time series.

Harmonic analysis was used to examine the contributions of the individual tidal constituents in the tidal signal for both water level and velocity. The analysis of the mooring observations was conducted using the T_Tide software package, which provides constituent coefficients and phase information as well as the associated error estimates for all astronomical constituents that can be distinguished given the duration of the time period [*Pawlowicz et al.*, 2002]. The resulting constituent amplitude coefficients and phases at the two sites were used to determine the relationship between velocity and water level as well as any spatial changes in the dominant constituents in Broad Sound. The harmonic parameters were used to generate a predicted tidal signal, which can be compared to the observed tidal signal and can be expressed as:

$$\eta(t)=\eta_o+\sum_{n=1}^{k} a_n\cos\left(\omega_n t-\phi_n\right) \tag{1}$$

where $\eta(t)$ can represent the predicted tidal signal or one of the two orthogonal components of the currents, $\eta_o$ is the predicted mean value, n is the individual tidal constituent, k is the total number of harmonic constituents, $a_n$ is the amplitude coefficient, $\omega_n$ is the frequency of the harmonic constituents, and $\varphi_n$ is the phase of the harmonic constituents. A similar method was used to calculate tidal ellipses from the current vector time series as described in *Pawlowicz et al.* [2002].

Correlation analysis was applied to the low-frequency time series to examine the relationships between velocities at different site locations as well as between wind fluctuations and both along-sound velocity and water level. Due to the strong relationship between wind forcing and subtidal currents (discussed below), additional analysis on the water column structure was conducted using the net flux ratio (NFR). As described by *Whitney and Codiga* [2011], the NFR is defined as $FR=\left|\int_{-h}^{\eta} v_{dm}\, dz\right| \Big/ \int_{-h}^{\eta} |v_{dm}|\, dz$, where $\eta$ is the surface (assumed to be zero in the subtidal calculations), $-h$ is the depth at the mooring site, and $v_{dm}$ is the subtidal along-sound currents with the mean removed. Mean currents are removed from the low-pass signal in order to limit the impact of nonwind-induced circulation patterns (mean local wind forcing was less than 2 m $s^{-1}$). The resulting demeaned subtidal current measurements are extrapolated to the surface and bottom following *Shearman and Lentz* [2003]. NFR values range between 0 and 1 where 0 represents a balanced horizontal flux through a unit cross section (i.e., dominated by vertical layering) and 1 represents unidirectional flux through a unit cross section (i.e., dominated by lateral alignment). The overall character of the wind response can be represented with the lateral alignment index (LAI) which averages the net flux ratio across a given transect [*Whitney and Codiga*, 2011]. Given the available measurements, the LAI cannot be calculated for Broad Sound, however, the NFR at each site, in conjunction with the survey measurements, does provide some information about the structure of the wind response.

With regard to the ship survey, a simplified harmonic analysis using only the M2 constituent, due to the short duration of the survey, was applied to the measurements from which tidal amplitudes (major and minor components) and a constant (subtidal signal) were obtained from the depth-averaged observations and at individual bin depths. Both the resulting velocity and the CTD (temperature, salinity, and density) signals were interpolated using a shape-preserving piecewise cubic fit to a 0.5 m (vertical) $\times$ 100 m plane along the transect.

## 3. Results

The instantaneous water level and velocity observations (not shown) are dominated by tidal (i.e., high frequency) processes. The relative importance of the tidal and low-frequency signals to the sites' characteristics were compared through the variance (Table 1) which clearly showed the dominant fluctuations in the system occur at high frequencies. At Portland, the tidal signal represented virtually all of the variance of the water level time series and was similar to the partitioning of the variances of the depth-averaged velocities at sites B1 and B2. Although the low-frequency contribution to the total depth-averaged variance is small, these time scales can be important for the transport of material in coastal regions. The low-frequency signal becomes increasingly important when considering the vertical shear, where the low-frequency variance of the surface-to-bottom velocity difference in the along-sound direction was more than a third and more than half of the high-frequency shear at sites B1 and B2, respectively.

**Table 1.** Variance Distributions for the Depth-Averaged Velocity and Surface-to-Bottom Velocity Difference (Labeled as "Shear") at the Mooring Sites and for Water Level at Portland During Period 3 (17 September to 15 November 2013)[a]

| | Instantaneous | Low-Pass | % | High-Pass | % |
|---|---|---|---|---|---|
| *Site B1* | | | | | |
| Along-sound ((cm s$^{-1}$)$^2$) | 835.7 | 4.9 | 1 | 802.7 | 96 |
| Across-sound ((cm s$^{-1}$)$^2$) | 34.1 | 0.9 | 3 | 33.1 | 97 |
| Along-sound shear ((cm s$^{-1}$)$^2$) | 420.3 | 109.8 | 26 | 321.3 | 76 |
| Across-sound shear ((cm s$^{-1}$)$^2$) | 132.0 | 8.7 | 7 | 121.9 | 92 |
| *Site B2* | | | | | |
| Along-sound | 396.2 | 0.6 | $<1$ | 393.2 | 99 |
| Across-sound | 19.2 | 1.0 | 5 | 18.1 | 94 |
| Along-sound shear | 159.3 | 53.2 | 33 | 103.6 | 65 |
| Across-sound shear | 119.6 | 16.3 | 14 | 102.8 | 86 |
| Portland | | | | | |
| Water level (m$^2$) | 1.1 | 0.0 | $<1$ | 1.0 | 99 |

[a]The percent values in the table represent the variance contribution relative to the instantaneous variance.

## 3.1. Tidal Variability

### 3.1.1. Mooring Observations

The tidal water level observations at Portland and the tidal depth-averaged velocity observations were dominated by semidiurnal fluctuations that had a clear spring/neap modulation (Figure 2). While along-sound currents clearly dominated the tidal flow with amplitude fluctuations between 30 and 60 cm s$^{-1}$, the across-sound currents were not insignificant, being about 20% of the along-sound currents. There was also notable spatial variability in the magnitude of the tidal velocities with site B1 having stronger currents than site B2. Details of the tidal water level and depth-averaged along-sound velocity characteristics during a typical spring tide are shown in Figure 3. The along-sound velocity at both sites was relatively sinusoidal with a dominate semidiurnal frequency that was typical of a standing wave relationship, where the maximum water level was accompanied by nearly zero along-sound flow and the maximum along-sound ebb/flood current was accompanied by a zero crossing of the water level.

The observed patterns in the tidal signal were quantified using harmonic analysis. The harmonic constituents between the two locations provided information about the spatial and temporal changes that occur as the tide propagates through Casco Bay. As expected, water level was primarily controlled by the M2 tidal constituent, but there were small contributions from other constituents such as the S2 and N2, which lead to a spring/neap modulation. In addition, the diurnal constituents in the system had only a small contribution to the tidal signal given that the system Form number (F) was less than 0.16, where F is the ratio of the sum of the amplitudes of the two main diurnal constituents (K1 + O1) to that of the semidiurnal constituents (M2 + S2) [*National Ocean Service*, 2000]. With regard to the tidal currents, the M2 signal was dominant with depth-averaged along-sound

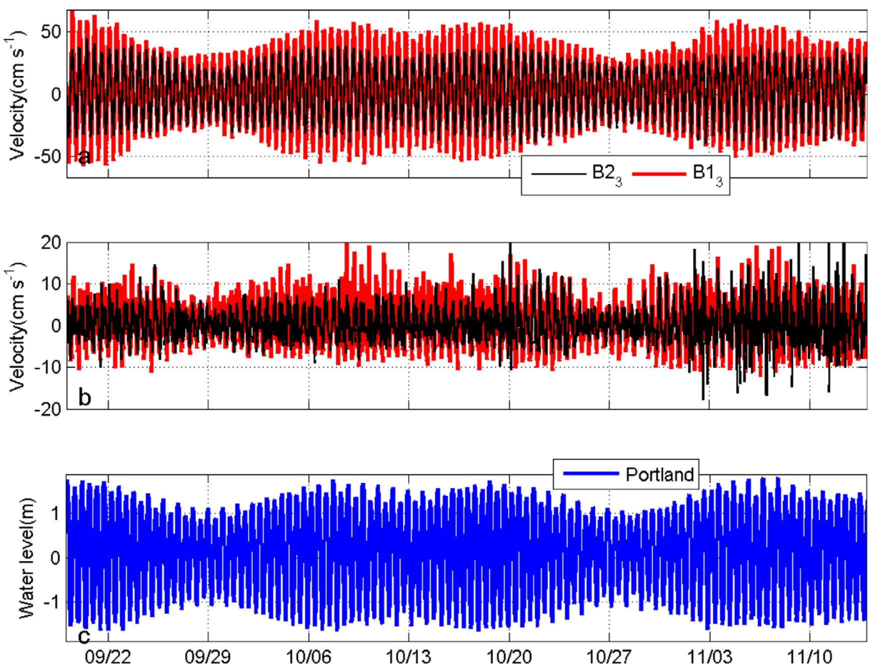


**Figure 2.** The high-pass signal from Period 3 ($_3$) showing the (a) depth-averaged along-sound and (b) across-sound velocity for mooring sites B1 (red), B2 (black), and (c) water level from Portland. Note the scale change of the *y* axis in Figures 2a and 2b.

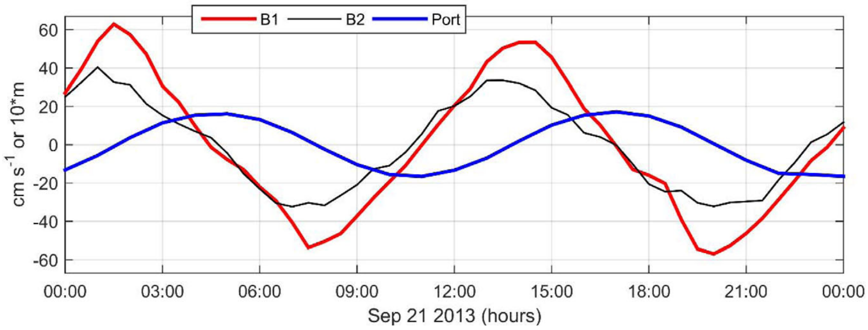


**Figure 3.** (a) The high-pass signal on 21 September showing the depth-averaged along-sound velocity for mooring site B1 (red), site B2 (black), and water level from Portland (blue). Note the scale change of the *y* axis as well as the scaling of the water level observations by a factor of 10.

amplitudes of 38($\pm$1) cm s$^{-1}$ and 26($\pm$1) cm s$^{-1}$ at sites B1 and B2, respectively, demonstrating a decrease in the M2 tidal current strength by approximately 1/3 ($\sim$12 cm s$^{-1}$) going across Broad Sound from sites B1 to B2. There was almost no phase difference between the sites and there was a $\sim$90° offset from the M2 water level constituent at Portland, consistent with a standing wave. The M4 and M6 overtides represented minor contributions to the along-sound flow structure, being less than $\sim$7% of the M2 constituent. Interestingly, while the harmonic analysis represented the along-sound currents quite well (analysis captured greater than 97% of the high-pass variance), the across-sound currents were poorly described (analysis captured at most 74 and 38% of the variance at sites B1 and B2, respectively). The vertical structure of the tidal currents during slack tides was examined for kinematic patterns associated with tidal straining processes; however, clear patterns were not readily distinguishable (not shown).

### 3.1.2. Survey Observations

Observations from the ship-based survey across Broad Sound provided improved spatial resolution of the tidal velocity structure and the resulting hydrographic changes. Tidal ellipses of the M2 constitute derived from the depth-averaged currents at each station indicated the predominance of the major axis and relatively consistent orientations of the tidal fits (Figure 4). The station orientations, being generally in the 349°/169° direction, are similar to the tidal flows determined at the mooring. There was a significant gradient in the magnitude of the semidiurnal tidal currents with the amplitude decreasing with distance away from the west side of the transect, which was also consistent with the mooring analysis. Using the along-sound component of the velocity, the vertical structure of the tidal currents across the sound was captured (Figure 5a). In addition to the lateral differences in the velocity structure, changes in the vertical structure of the tidal magnitudes were evident with the slopes having somewhat larger vertical gradients than the deeper central region. Note the stronger amplitudes at stations 2 and 4 ($\sim$50 and 35 cm s$^{-1}$, respectively) in the survey measurements when compared to the mooring measurements result from the survey being conducted during a spring tide, for which the contributions of the other semidiurnal tides cannot be separated due to the short duration of the survey period. The phase of the semidiurnal tide has minor differences throughout the majority of the across-sound transect (Figure 5b). There was a notable phase shift of $\sim$10–20° at station 6 (i.e., the eastern most portion of slope) as compared to the main body of the sound. Density measurements over the tidal cycle at stations 2 and 5 are shown in Figure 6. The structure of the density on both the western and eastern slopes was generally similar with the surface-to-bottom difference on the order of about 0.5–1.0 kg m$^{-3}$. Interestingly, the flood tide was more stratified than ebb tide opposite to what is expected in typical estuaries that have a large freshwater source at the head. However, the depth-averaged density was still lower during ebb than flood, indicating the depth-averaged density increases with southward distance out of the estuary.

## 3.2. Mean Currents

To provide context for the subtidal fluctuations, the structure of the mean currents are first examined to determine their relative contribution to the subtidal signal. The mean currents at sites B1 and B2 demonstrated significant spatial differences across Broad Sound (Figure 7). In terms of along-sound circulation,

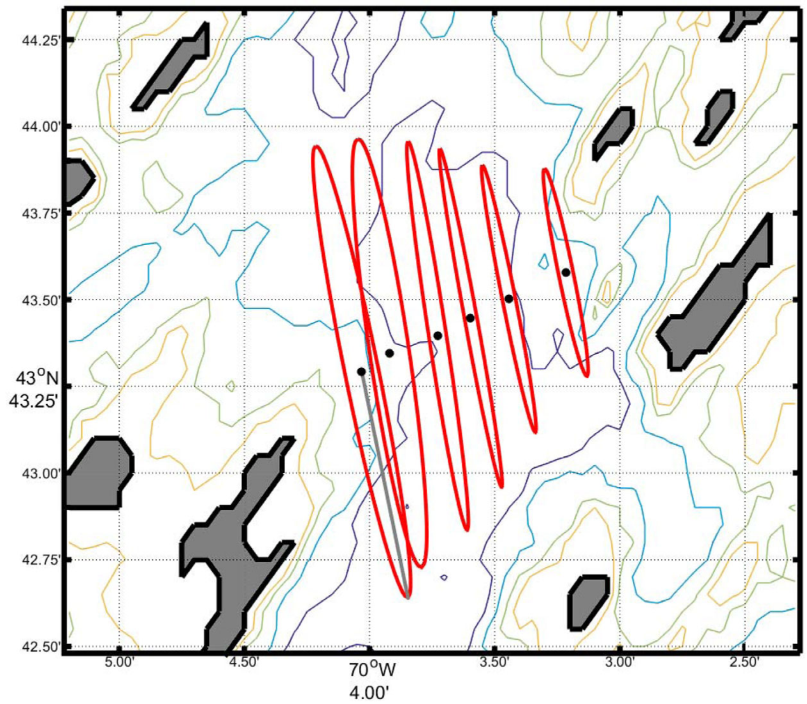


**Figure 4.** M2 tidal ellipses of the depth-averaged velocity at each station during the 21 September survey with the associated bathymetry (black contours are islands and color contours are the 5 m (orange), 10 m (green), 20 m (light blue), and 35 m (blue) isobaths). The black dot indicates the position of each station during the survey with station 1 (station 6) being furthest west (east) and the gray line in the station 1 tidal ellipse representing a velocity scale of 56 cm $s^{-1}$.

there was outflow (inflow) throughout the water column over the western (eastern) slope, clearly indicating strong lateral shearing; however, there was also some vertical shearing, with the western slope having slightly larger shear than the eastern slope, and the direction of the shear was consistent on both sides (i.e., both had increasing northward or northward trending velocities at depth). In terms of lateral circulation, the across-sound velocity structure indicated the presence of a net eastward flow across the sound. The velocities were of the same order of magnitude as the along-sound velocity, and the depth-averaged velocity was not zero. Furthermore, the lateral structure of the across-sound velocity indicated a confluent flow field throughout the water column, with the strongest currents on the western slope (site B1) decreasing to the weakest currents on the eastern shoal (site B2, Period 3).

Despite having only about 3 weeks of observations during Period 1, the velocity structure at site B1 was similar to Period 3 (not shown), and the structure of the upper layer at site B2 was quite similar to site B2 during Period 3, suggesting the mean profiles during Period 1 are a reasonable representations of the mean circulation for study period. As such, the profiles for site B2 during Period 1 will be considered to be the mean structure in the deepest point in the bathymetric cross section. The along-sound profile appeared to be an extension of the pattern observed at site B2 during Period 3, having inflow throughout the water column over the deepest point in the bathymetric cross section. Similarly, the across-sound structure was consistent with observations of the mean structure over the slopes as the profile in the deepest point in the bathymetric cross section was within the envelope of the confluent flow pattern observed between the slope sites. In addition, all three profiles had a near-bottom decrease in velocity, with the deep channel profile indicating a very weak reversal at the bottom.

### 3.3. Subtidal Variability

#### 3.3.1. Mooring Observations

The low frequency signals of wind and current velocities from the mooring in Broad Sound and water level at Portland are shown for Period 3 in Figure 8. The signals for wind, currents, and water level were characterized by oscillations on the order of a few days. The subtidal velocities at both sites had similar oscillations

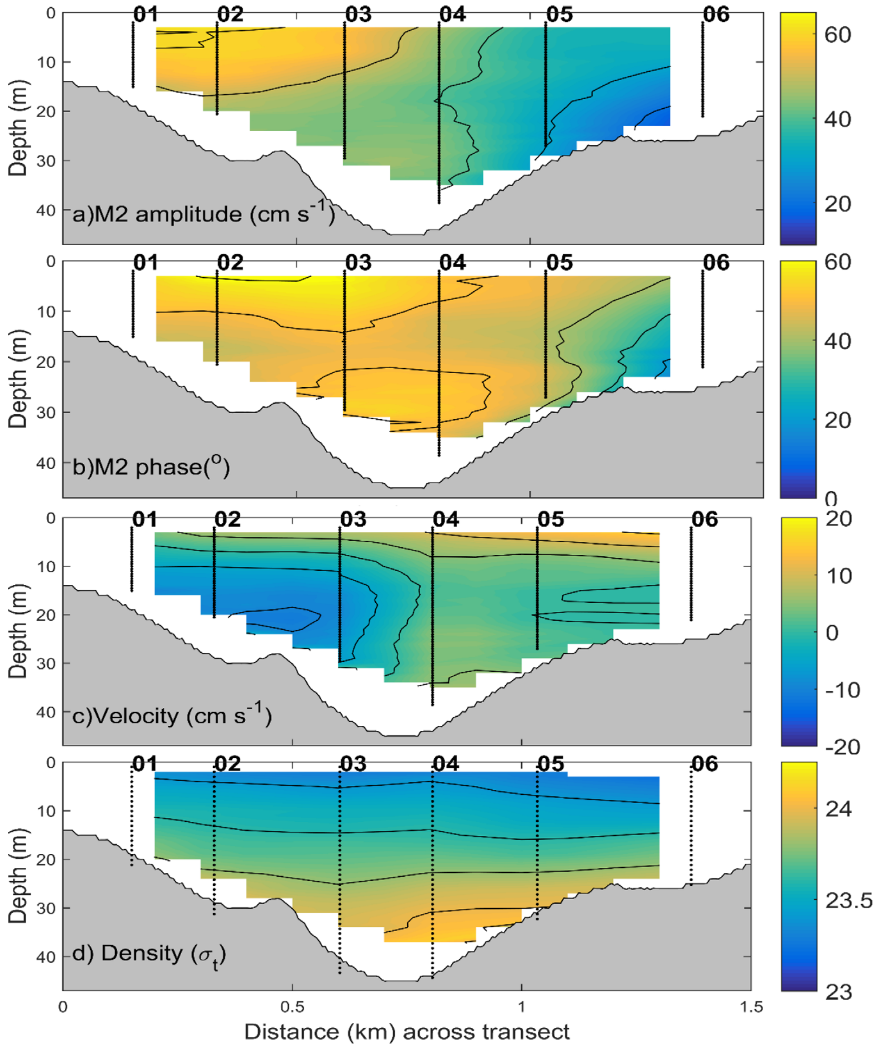


**Figure 5.** (a) M2 along-sound tidal amplitude, (b) M2 phase of the along-sound tidal current, (c) along-sound subtidal currents, and (d) subtidal density across Broad Sound during the 21 September ADCP/CTD survey. The station locations are indicated by the vertical lines. The mooring sites B1 and B2 were located near stations 2 and 4 during Period 1, respectively, and stations 2 and 5 during Period 3. The phase is relative to the start time of the first transect. The subtidal currents and density represent the mean conditions over the observed tidal cycle on 21 September, which occurred during the onset of an up-estuary wind event. The transect view is looking into the system with positive (negative) values directed into (out of) Broad Sound.

and vertical shear with outflow at the surface and inflow at depth (only the near-bottom current at site B2 are shown for clarity, site B1 is qualitatively similar) with occasional reversals (e.g., 22 September, 29 September, 7 October, etc.). The spatial relationship was quantified with correlations where the surface (near-bottom) currents had an r-value of 0.92 (0.64) with a lag of 3.5 (1.5) h (lag represents site B1 leading B2). Thus, the lateral fluctuations across Broad Sound at the subtidal time scale were similar throughout the water column. As noted in the description of the mean currents, the lateral shear between the two sites acts on a longer time scale. The vertical fluctuations between the surface and near-bottom were negatively correlated having values of $-0.81$ and $-0.72$ (with lags of 8.5 and 6 h) for sites B1 and B2, respectively. This demonstrates that the vertical structure of the horizontal velocity is strongly coupled, with the surface and bottom currents having opposing fluctuations on the slopes of Broad Sound. In terms of the depth-averaged subtidal flow, as indicated by the variance contribution of the depth-averaged subtidal signal (Table 1), these fluctuations were small ($\sim$3 cm s$^{-1}$ at B1 and $\sim$2 cm s$^{-1}$ at B2) and uncorrelated between mooring sites suggesting the vertically uniform current response associated with remote wind forcing is of limited importance in Broad Sound.

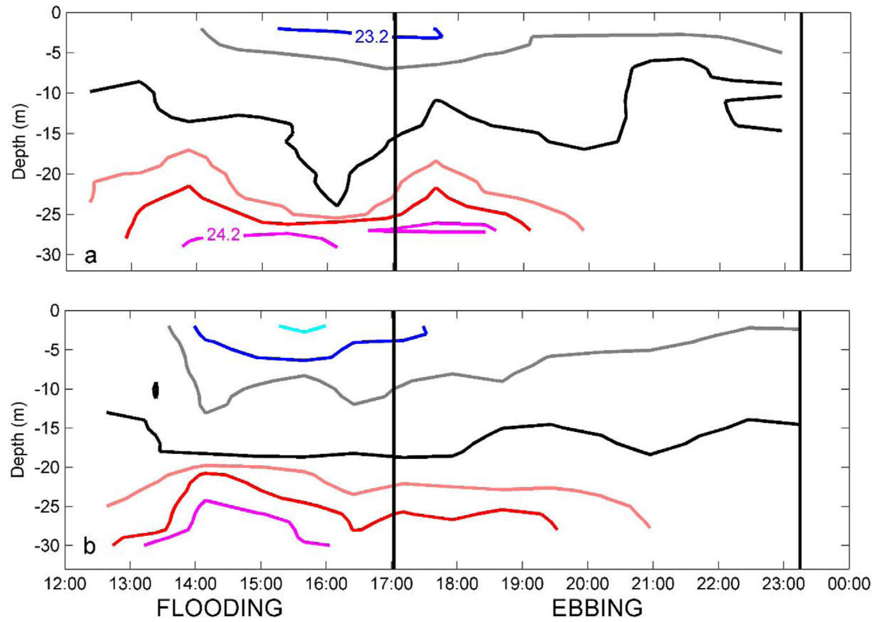


**Figure 6.** Density observations at (a) station 2 and (b) station 5 (see Figure 5) during the ADCP/CTD survey of Broad Sound on 21 September. The values associated with the contour colors are the same in both plots and occur at 0.2 $\sigma_t$ intervals. The vertical lines represent times of high and low tide, respectively. Note stratification is stronger during flooding conditions at both sites.

There were multiple strong wind events (>5 m s$^{-1}$) in the along-sound (AL) wind speed time series; however, these are not well correlated with the current velocity time series. This is particularly obvious during the second half of Period 3, as illustrated by the series of strong wind fluctuations during 20 October to

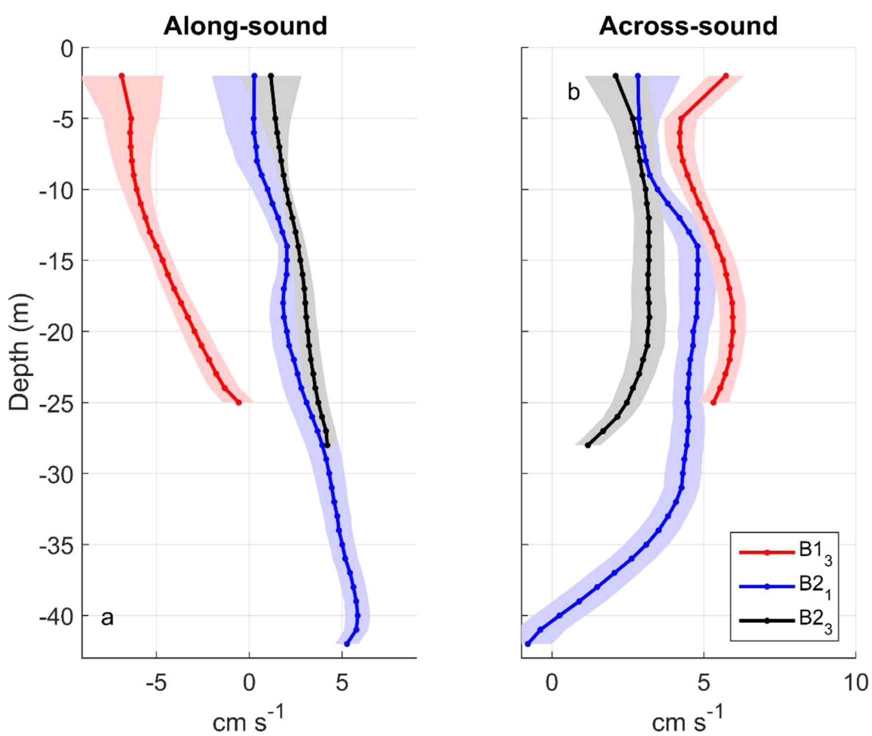


**Figure 7.** Structure of the mean (a) along-sound and (b) across-sound velocity during Period 3 at site B1$_3$ (red) and site B2$_3$ (black); and during Period 1 for site B2$_1$ (blue). Note the site B2$_1$ profile was determined from a 3 week period in August to September. Positive (negative) values are inflow (outflow). The shading around each profile indicates the standard error associated with the mean flow.

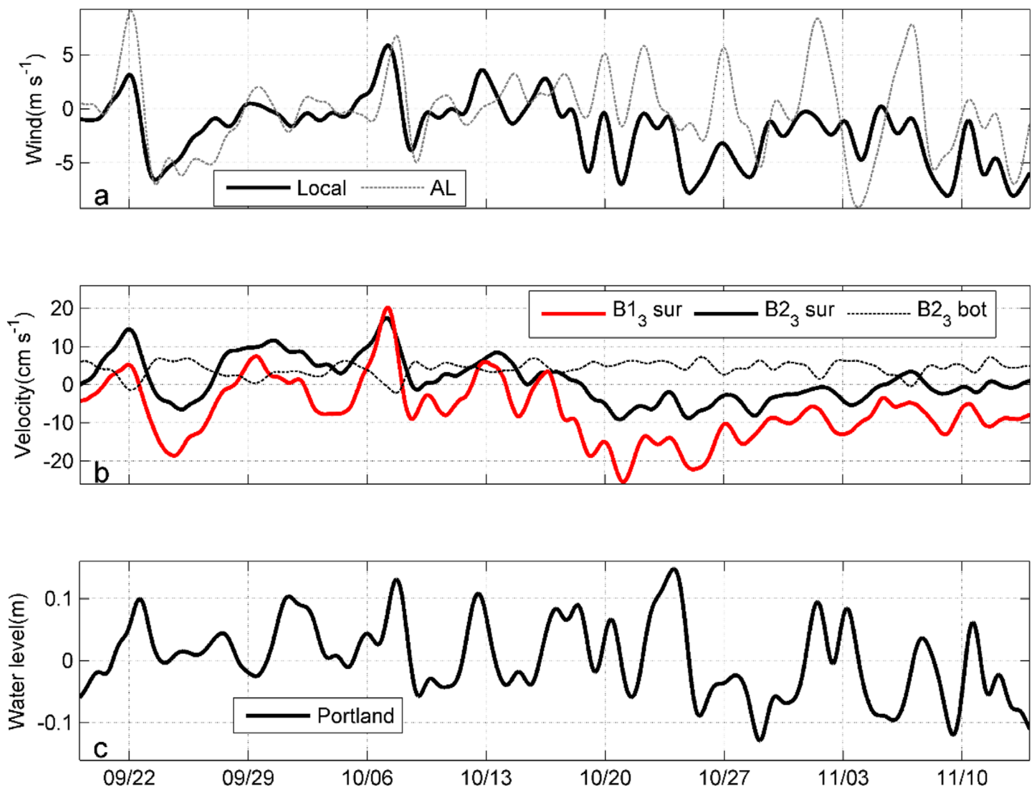


**Figure 8.** Subtidal signal during Period 3 of 2013: (a) wind speed at site B1 for the along-sound (AL) direction and the direction of highest correlation with the current shear (i.e., local), (b) near-surface along-sound current at site B1 (red) and B2 (black) and near-bottom currents (black dashed) at site B2, and (c) water level at Portland. The positive (negative) along-sound wind and current is up-estuary (down-estuary) and the positive local wind direction is 280°T.

8 November that had no similar response in the velocity time series. The direction of maximum correlation between the local wind forcing and the along-sound currents was determined by examining the correlation between the surface-to-bottom velocity difference with wind components spanning all 360° at 5° intervals. The resulting angle of maximum correlation was 280° and 285°T ($r = 0.77$ and 0.71 with lags of 4 and 7 h) for sites B1 and B2, respectively, meaning wind blowing along a west-northwest/east-southeast orientation is associated with the two-layer flow over the slopes of Broad Sound. The high r-values indicate that more than 50% of the subtidal fluctuations in the surface to bottom velocity difference can be explained with local wind forcing (black line, Figure 8a). Additional details of the water column response to low frequency wind forcing are demonstrated with the vertical structure of the correlation coefficient and their associated time lags (Figure 9). At both sites B1 and B2, the correlations are high ($>0.5$) for the upper and lower portions of the water and have similar time lags with the surface responding faster ($\sim$5–10 h) than the lower layer ($\sim$10–15 h). Between 9.5 and 15.5 m depth, the correlations were either insignificant and/or had lag times that were physically unrealistic. This is indicative of the transition region where current response to wind forcing changes direction (i.e., correlations are poor in this region of the water column due intermittent changes in the depths of the response layers). Correlation comparison between wind components and water level in Portland indicated a maximum correlation angle of 295°T ($r = 0.60$ with a lag of 13 h) which was similar to the current response. Water level responds to local wind forcing by increasing (deceasing) during up (down)-estuary wind events, which is consistent with the current shear response to wind.

The shorter time series from Period 1 provides insight on the relationships between the deepest point in the bathymetric cross section and slopes (Figure 10). In many respects, the characteristic behaviors between the slopes and deepest point in the bathymetric cross section are quite similar. At the surface (Figure 10b) and across much of the lower portion of the water column, the velocity fluctuations were similar between sites. This is also true of the response to wind forcing where the correlation between wind and upper-layer shear (difference between the surface velocity and the 28 m depth velocity) was correlated with a wind

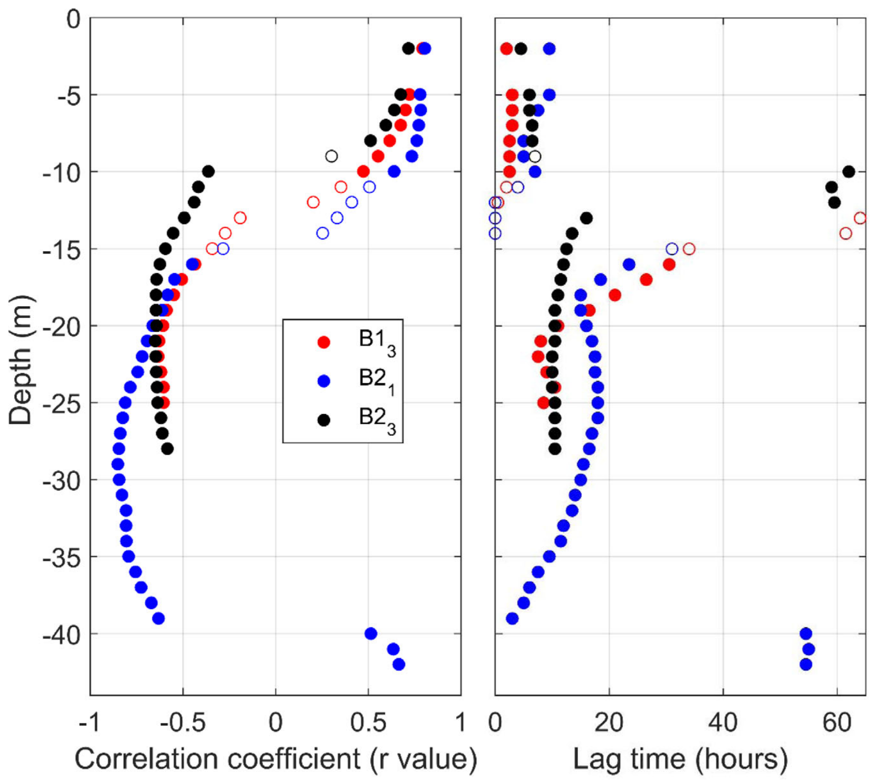


**Figure 9.** (a) Correlation coefficient and (b) time lag of the maximum correlation between local wind and the along-sound current velocity throughout the water column during Period 1 at site B2 (blue circle) and Period 3 at sites B1 (red circle) and B2 (black circle). Each circle represents a velocity bin depth and open circles are not significant.

angle of 285°T (r = 0.86 with 11 h lag). The overall structure of the wind response at both sites was similar to Period 3 with the transition from positive correlations at the surface to negative values at depth occurring at similar depths (~10–15) (Figure 9; site B1 of Period 1 not shown).

Some potential differences arose in the currents near the bottom of the deepest point in the bathymetric cross section, where correlation analysis during Period 1 reveal positive correlations ($r > 0.5$) between wind and current beginning at 40 m and extending to the deepest available depth (Figure 9). These correlations also had longer lag times (lag ~55 h). Given the relatively short duration of Period 1 (25 d) and limited possible forcing mechanisms (section 4.3), these correlations should be viewed cautiously, but suggest the response to wind forcing at the near-bottom of the deepest point in the bathymetric cross section is notably altered from that on the slopes (i.e., the near-bottom of the deepest point in the bathymetric cross section is oppositely directed when compared to that of the near-bottom on slopes and has a longer response time scale). Note fluctuations in the near-bottom of the deepest point in the bathymetric cross section are modulations of deep inflow, not reversals in flow direction (i.e., the near-bottom of the deepest point in the bathymetric cross section was always flowing inward; Figure 10b).

### 3.3.2. Survey Observations

Observations from the ship survey across Broad Sound provide improved spatial resolution of the subtidal response of the system during a reversal event (i.e., up-estuary wind event). This spatial structure of the subtidal current was consistent with the mooring observations. Over the slopes, the current velocity consisted of a sheared two-layer system, with inflow at the surface and outflow at depth (Figure 5c). As seen in the mooring velocity measurements, the outflow (inflow) was stronger on the western slope (eastern slope). Furthermore, the velocity structure of the deepest point in the bathymetric cross section had inflow at the surface, a strong reduction at middepth (being nearly zero) and inflow near the bottom (similar to the behavior of site B2 during Period 1 when it was located in the deep channel). The subtidal hydrographic structure was consistent with a weakly stratified water column (surface-to-bottom difference of 0.5–1.0 kg

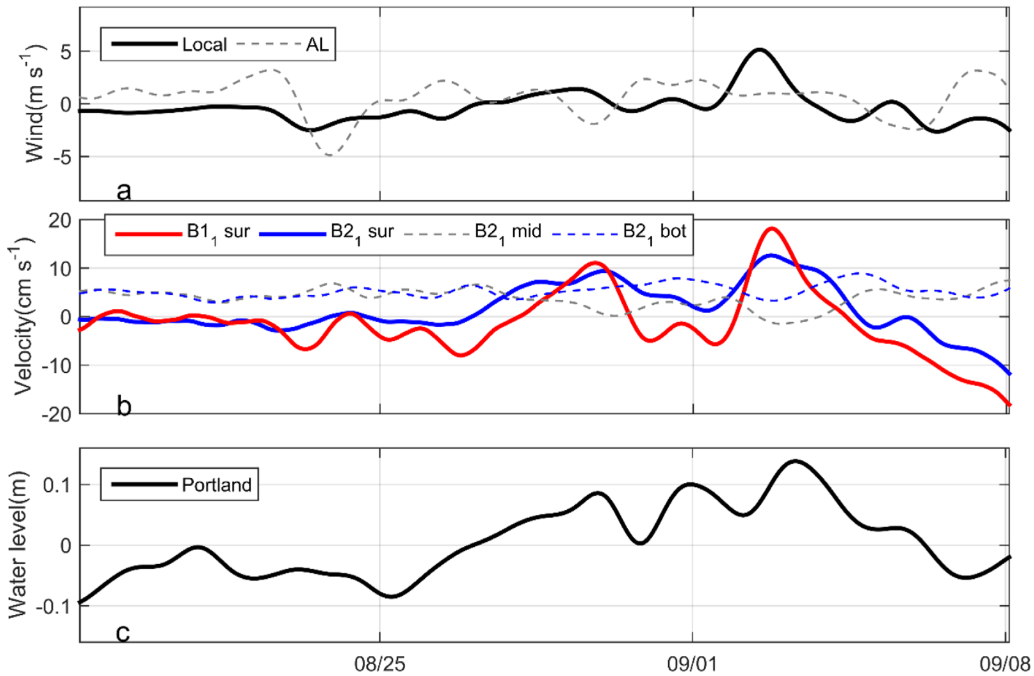


**Figure 10.** Subtidal signal during Period 1 of 2013: (a) wind speed at site B1 for the along-sound (AL) direction and the direction of highest correlation with the current shear (i.e., local), (b) near-surface along-sound current at sites B1 (red) and B2 (blue) and middepth (28 m) and near-bottom currents (gray and blue dashed, respectively) at site B2, and (c) water level at Portland. The positive (negative) along-sound wind and current is up-estuary (down-estuary) and the positive local wind direction is 280°T.

m$^{-3}$ over the slopes and deepest section, respectively) with some limited lateral variability (Figure 5d). The eastern side of the deepest point in the bathymetric cross section had the highest density in the cross section while the eastern slope had slightly deeper fresh water penetration with the 23.4 $\sigma_t$ contour being at ~7 m depth on the east compared to the ~ 2 m depth on the west.

## 4. Discussion

### 4.1. Tidal Processes

The tidal characteristics at the moorings in Broad Sound are generally consistent with a barotropic standing wave system. This is evident in the vertical structure of the tidal constituents (i.e., deceased amplitude with depth, Figure 5a) and the approximate 90° shift between the water level and velocity. Furthermore, the estimates of the M2 phase across the sound are generally spatially uniform with minimal vertical variability (stations 1–5), which is also consistent with a barotropic standing wave response (Figure 5b). There was some shift in phase structure at the east edge of the transect (i.e., station 6). However, the lateral change in the velocity amplitude was much more notable (i.e., decreasing magnitude from west to east). In an idealized two-dimensional estuarine cross section, where the coastline and bathymetry are clearly defined, barotropic tidal forcing is expected to generate the strongest velocities in the deepest point in a bathymetric cross section [e.g., *Huijts et al*., 2006; *Lee et al*., 2013] due to the more limited frictional effects on the flow. This is clearly not the case in Broad Sound where the complex bathymetry and open boundary provide the potential for other processes to alter the tidal velocity structure. For example, headlands and their associated subsurface extensions are known to intensify tidal currents due to the Bernoulli effect derived from the development of a pressure minimum near the tip of a headland [*Signell and Geyer*, 1991]. While the results of *Signell and Geyer* [1991] are not clearly applicable in this case, the western stations of the transect (particularly, stations 1 and 2) are located on the slope of small subsurface outcropping which could be amplifying the flow in a similar manner. An equally plausible explanation for the lateral variability in the tidal currents could result from tidal interaction with the surrounding water bodies. The relatively open nature of Broad Sound allows for tidal exchanges and interactions in both the along and across-sound directions, leading to potentially complex flow patterns.

Due to the importance of density gradients on vertical shear, the lack of density measurements during most of the mooring deployment presents a significant limitation on interpreting the intratidal velocity structure observed during the study period. Previous hydrographic observations [*Sinnett*, 2012, Figure 5] and observations from this study indicate Broad Sound is a weakly stratified system (i.e., surface-to-bottom density difference $\sim$0–2 kg m$^{-3}$). However, multiple potential sources of fresh water as well as complex bathymetric features (i.e., spatially varying bottom boundary layers/mixing throughout the system) presents an estuarine setting where the density gradients are likely to have significant spatial and temporal variability.

This variability is captured, to some extent, in the hydrographic measurements from the ship survey, which observed increased stratification on flood rather than ebb (Figure 6). Several studies have documented this hydrographic behavior and have generally attributed this density structure to advective transport [*Scully and Friedrichs*, 2007, *Scully and Geyer*, 2012; *Becherer et al*., 2011; *Basdurak and Valle-Levinson*, 2013]. For example, *Scully and Friedrichs* [2007] found that the timing of laterally advected stratified water from the deep channel region of the James River caused this behavior. Similarly, *Becherer et al*. [2011] noted the observed increase in stratification on flood at their study site likely resulted from the lateral advection of a vertically stratified water mass.

Similar advective processes are likely important in Broad Sound. Advection of a more stratified offshore water mass is a reasonable possibility, as it has been shown that discharge from the Kennebec-Androscoggin River system can generate a reverse buoyancy gradient in outer Casco Bay [*Janzen et al*., 2005; *Xue and Du*, 2010] and the New Meadows River estuary (to the northeast of the study region) [*Kistner and Pettigrew*, 1999] during the period of high discharge. Additionally, the complex bathymetry (i.e., irregular shoals and narrow passage ways) shoreward of the transect in Broad Sound would be expected to drive more mixing in the shallower waters of inner Casco Bay. Consequently, the observed density structure likely results from the advection of a weakly stratified offshore water mass on flood and a more well-mixed inner estuary water mass on ebb (Figure 6). Hydrographic observations during a survey on 21 July 2013 was also consistent with this pattern (not shown).

To summarize, there are several likely mechanisms that can generate temporal and spatial variability in the intratidal density gradients in Broad Sound, which will in turn will lead to variability in the intratidal velocity structure. Tidal straining and intratidal lateral circulation are clearly important in subtidal dynamics of certain types of systems (e.g., systems with strain-induced periodic stratification) [e.g., *Simpson et al*., 1990; *Lerczak and Geyer*, 2004; *Huijts et al*., 2009; *Cheng et al*., 2010, 2011; *Burchard and Hetland*, 2010; *Burchard et al*., 2011]; however, the relative importance of asymmetries in the intratidal velocity shear on the mean circulation in a weakly stratified, relatively deep, meso-tidal system is unclear. *Geyer and MacCready* [2014] found that organizing estuarine systems by their fresh water Froude number ($F_{fr}={U_R}/{(\beta g \Delta s H)^{1/2}}$ where $U_R$ is river discharge, $\beta$ is 7.7 $\times$ 10$^{-4}$, $\Delta$s is the typical surface to bottom salinity difference, and H is the water depth in an estuary) and Mixing number ($M=\sqrt{C_D U_T^2 / \omega N_0 H^2}$, where $C_D$ is a drag coefficient, $U_T$ is the tidal velocity, $\omega$ is the tidal frequency, and $N_o$ is the buoyancy frequency for maximum top-to-bottom salinity variations) create a parameter space, in which the relative importance of asymmetric tidal mixing to the subtidal dynamics can be assessed. The fresh water Froude number ($F_{fr}$) represents the ratio of the net velocity due to river flow to the maximum possible frontal speed, whereas the mixing number (M) represents the ratio of the tidal time scale to the vertical mixing time scale. As the freshwater Froude number and the mixing number decrease, so does the relative importance of asymmetric tidal mixing in the subtidal dynamics.

In terms of the freshwater Froude number, sources of fresh water discharge are limited to a few small rivers that feed into inner Casco Bay in several locations, of which the Royal and Presumpscot Rivers are the largest contributors. Combined, these two primary sources of discharge have an annually averaged, mean daily flow rate of less than 40 m$^3$ s$^{-1}$ [*Hodgkins*, 1999] which suggests $U_R$ should be relatively small. In addition, the surface-to-bottom salinity difference observed at these sites is typically on the order of 1–2 psu, although there are short-term events during which values exceed this difference. Given this range of values, the freshwater Froude number of Broad Sound is expected to be small (O(0.01–0.0001)).

In terms of mixing number, the water depth ($\sim$30 m) and the tidal currents ($U_t \sim$ 0.35 m s$^{-1}$) in Broad Sound yield a value on the O($\sim$0.3–0.4). It is important to note that the M values will fluctuate to some degree with the spring-neap modulation in the tidal velocity strength as well as with seasonal stratification. Consequently,

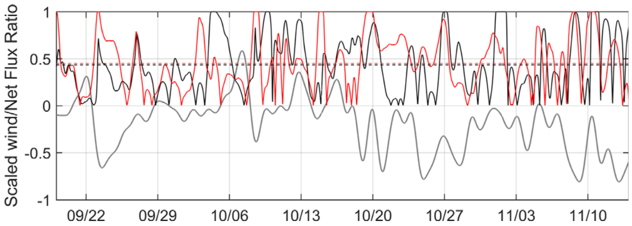


**Figure 11.** Times series of the net flux ratio (NFR) of the demeaned velocity at sites B1 (red) and B2 (black) and scaled local wind (gray) during Period 3. The dashed horizontal lines are the mean NFR for B1 (red) and B2 (black). The local wind forcing (m s$^{-1}$) is scaled by a factor of 0.1.

Broad Sound would be expected to span the fjord/bay boundary in the $F_{fr}-M$ parameter space. Consequently, the overall depth of the system and moderate tidal currents are expected to limit the role of asymmetric tidal mixing in driving subtidal circulation, as such, the system should be governed, in large part, by baroclinic pressure gradients (additional discussion in section 4.3).

### 4.2. Wind Forcing

The subtidal variability throughout the water column is dominated by local wind forcing as indicated by the correlation analysis. Over the slopes, the mooring observations indicated surface wind forcing driving flow into or out of the estuary at the surface with a return flow at depth. This response is consistent with inflowing (outflowing) water generating a barotropic pressure gradient (indicated by positive wind/water level correlation), which forces a return flow in the lower layer. While there is lateral shear between sites B1 and B2, the high positive correlation between the surface at both sites as well as between the surface and near-bottom at both sites shows the subtidal variability is very similar at both sites and the lateral velocity difference between the sites results from a process acting over longer time scales than the wind response (discussed in section 4.3).

The structure of the wind response at each site can be further examined with the net flux ratio (NFR) which quantifies the relative amount of vertical or lateral structure by comparing the transport to the overall volume flux (per unit lateral distance) through the water column as described in section 2. Time series of the NFR at both sites during Period 3 showed large variations in the structuring of the water column flow (Figure 11); however, the average values were less the 0.5, indicating a tendency favoring vertical layering at the transect across Broad Sound. The variability observed in the NFR time series (value fluctuations between 0 and 1) are, in part, due to other forcing processes not addressed by simply removing the mean profiles and do not always represent the wind response (e.g., during periods of weak winds or barotropic adjustment during relaxation periods postwind forcing). Consequently, the mean NFR values represent a coarse estimate of the structure of the wind response, but many of the individual wind events tended to be lower than the mean. This was particularly apparent during the ship survey period (21 September) when the values at sites B1 and B2 were less than 0.2.

The subtidal observations from the ship-survey represent a good illustration of the velocity structure under up-estuary wind forcing during moderate wind conditions and are consistent with the velocity structure that would be expected based on the low NFR values from the mooring sites (i.e., vertically sheared flow). This is clearly evident over the sloping edges of the transect (e.g., stations 1, 2, 3, and 6) where there is inflow at the surface and outflow at depth. The inflow observed in the deepest section of the transect likely resulted from wind forcing requiring a longer response time to overcoming the stronger baroclinic forcing in this deeper region. The tendency for vertical shearing over the deeper region of the sound is supported by NFR values for site B2 during Period 1 which had a mean value of 0.41 (not shown). This is consistent with the values at sites B1 and B2 during Period 3 (site B1 had a slightly higher value of 0.6 during Period 1).

Interestingly, the local response to wind forcing is not consistent with a wind direction directly along the axis of Broad Sound. Rather, the system is clearly responding to wind forcing orientated along an east-southeast/west-northwest direction rather than the approximate north/south orientation of Broad Sound (angles of maximum correlation were approximately 280–285°T). This response is more consistent with a wind forcing associated with the large-scale orientation of the Casco Bay system, i.e., 310–320°T. The response to an off-axis wind stress is likely related to the geometry of the system. Atypical from many estuarine systems, inner Casco Bay is much wider than it is long (width-to-length aspect ratio of $\sim$2), which prevents Broad Sound from being dynamically long enough for direct along-axis forcing to be an effective wind direction. An additional contribution to the flow structure may be derived from a time-dependent Ekman response with surface flow being directed to the right of the wind (i.e., the up-sound direction for west-northwestward winds) and the resulting bottom return flow to the left (i.e., the down-sound direction for west-northwestward winds). The relatively open nature of Broad Sound (i.e., its boundaries are not defined by continuous coastlines) could promote direct wind forcing of surface water across Broad Sound, originating from either side of the sound as well as from transport associated with other passageways that connect inner and outer Casco Bay.

Additionally, the mooring observations during Period 1 at site B2 reveal that near-bottom currents in Broad Sound respond differently than the near-bottom currents on the slopes. The near-bottom fluctuations in the deep channel are positively correlated with the wind and surface currents. The longer lag time (~2 days) associated with the deep-sound bottom response to wind forcing also suggests the process driving these fluctuations is different than the two-layer flow in the upper layer of the sound. It is speculated that this results from alterations in the along-sound baroclinic pressure gradient, which is being modulated by the local wind forcing. For example, during up-estuary events, the relatively short along-sound length of the system allows fresher surface water to be downwelled at the head of the estuary (where the water level is being setup), leading to an increase in the along-sound density gradient and increasing the inflow at the bottom. Alternatively, the flow reversal at middepth (or at the bottom over the shoals) could lead to a straining of the horizontal density gradient at depth, sharpening (weakening) the gradient during up (down)-estuary events. Given the limited sample size (i.e., Period 1 is only 25 days) and limited forcing measurements (i.e., no time series of density gradients), the robustness of the observed correlations should be examined in future work.

### 4.3. Role of Coriolis

Coriolis forcing has been shown to be important at both tidal and subtidal frequencies in estuarine dynamics. Focusing on longer time scales, aspects of the system can be put in context of the framework presented by *Valle-Levinson* [2008] which examines the structure of exchange flow in density-driven systems and the role of Coriolis by comparing the Kelvin and Ekman numbers. The Kelvin number, defined as $W/R_i$ where W is the width of the estuary and $R_i$ is the internal radius of deformation, represents the dynamical width of the system [*Garvine*, 1995]. When K is greater than 1, a system is dynamically wide and Coriolis force plays a dominant role in organizing the lateral along-channel velocity structure. The vertical Ekman number, defined as $A_z/fH_o^2$, where $A_z$ is the vertical eddy viscosity, f is the Coriolis parameter, and $H_o$ is the maximum depth, represents the dynamical importance of friction in the system. In systems where Ek is greater than 1, friction dominates over rotation. In Broad Sound, the Kelvin number can be estimated using the system width (~2500 m), density (~1024 kg m$^{-3}$), vertical density difference (~1 kg m$^{-3}$), layer depth (~10 m), and Coriolis parameter ($1.0 \times 10^{-4}$ s$^{-1}$) and is approximately 0.8. A similar, but slightly higher value (K ~ 0.9) was determined by *Sinnett* [2012]. For estimates of the Ekman number, $A_z$ must be determined. While this is not trivial, a simplified method for estimating $A_z$ has been put forth by *Kasai et al.* [2000] for which $A_z = \frac{u_*^2}{200f} F(Ri)$ where $u_* = \sqrt{C_D} U$ is the friction velocity (U is the magnitude of the tidal velocity) and F is the function, $F = (1+7Ri)^{-1/4}$ where Ri is the Richardson number ($\frac{\Delta\rho}{\rho_o}\frac{gh}{U^2}$, where $\Delta\rho$ is the density change over depth h, g is the gravitation acceleration, and $\rho_o$ is the reference density). Letting $\Delta\rho = 1$ kg m$^{-3}$, h = 10 m, $\rho_o = 1024$ kg m$^{-3}$, and U = 35 cm s$^{-1}$, $A_z$ is on the order of 0.01. Using this value of $A_z$, f at Broad Sound, and $H_o$ ~ 40 m, the Ek is approximately 0.06. Both the Kelvin number and the Ekman number indicate that Coriolis forcing will have a dynamical role structuring the circulation in the system. In a density-driven, positively buoyant estuary (i.e., low density water at the estuary head) where Coriolis force is important, lower density water will accumulate on the left side of a cross section (looking landward), generating lateral sheared flow with outflow on the left and inflow on the right. The three mooring locations show significant lateral shear across the estuary, with net outflow on the western slope and inflow over the deepest point in the bathymetric cross section and eastern slope, consistent with the influence of Coriolis. These observations are consistent with numerical modeling work in Casco Bay and the greater coastal region that noted monthly mean currents during the spring of 2004 and 2005 that had a laterally sheared flow structure in Broad Sound (H. Xue, personal communication, 2014). The vertical shearing of the profiles is strongest on the east side, but is consistently negative across the sound, indicating the mean flow structure is not entirely dominated by Coriolis forcing. This lateral and vertical shear structure has been observed in other systems in which Coriolis forcing is important. For example, *Codiga and Aurin* [2007] observed flow features in eastern Long Island Sound that are similar to those in Broad Sound. Furthermore, while idealized dynamics from straight estuaries may not be completely applicable to the bathymetrically complex region associated with Broad

Sound, the flow structures are quite similar to the work of *Valle-Levinson* [2011] which summarizes previous work on the transverse structure of density-driven subtidal circulation by organizing the results of an analytical modeling effort using Kelvin and Ekman numbers. The observational results of this study compare very well to the analytical results (Figures 11g and 11h) [*Valle-Levinson*, 2011]. In addition to the observed along-sound velocity structure being well represented in nondimensional parameter space, the structure of the observed across-sound circulation is also similar. The confluent across-sound velocities (Figure 10) are relatively consistent with the analytical solutions presented in *Valle-Levinson* [2011]. Despite some differences (i.e., analytical solutions have outflow across the entire upper layer unlikely the mooring observations), the qualitative similarities indicate density-driven circulation is a significant component of the mean circulation. While a number of recent modeling results have demonstrated that lateral advection and/or tidal straining can be a primary driving force in the development of vertically sheared estuarine exchange flow, their role in a dynamically deep and/or wide systems, where Coriolis forcing significantly modulates the flow structure needs further research.

## 5. Conclusions

Mooring and ship survey measurements were used to characterize the velocity and hydrographic structure in Broad Sound, a subsystem of Casco Bay, ME. At tidal time scales, the system is dominated by a barotropic semidiurnal standing wave with a west to east decrease in tidal amplitude and relatively minimal phase change across the majority of the transect (the exception being station 6). The system stratification was generally weak (vertical differences of 0.5–1.0 kg m$^{-3}$), laterally uniform, and stronger during the flood phase. The observed increase in stratification during the flood is hypothesized to result from stronger offshore stratification. The mean circulation had strong lateral shear with inflow throughout the water column over the deepest point in the bathymetric cross section and eastern slope and outflow throughout the water column over the western slope. There was also vertical shearing of the horizontal velocities across the sound with stronger northward or northward trending velocities at depth. The structuring of the observed mean circulation was influenced by Coriolis due to the system depth (via reduced friction; i.e., low Ekman number) and weak stratification (via short deformation radius), despite the physically narrow width of the system ($\sim$2500 m). Unfortunately, the relative strength of the gravitational circulation and other potential contributors, such as nonlinear advection and asymmetric tidal mixing, cannot be determined from these observations. However, the nondimensional scaling of the system characteristics (i.e., $F_{fr} < 1$, $M < 1$, and $K \sim$ 0.5–1) suggest these processes are likely to be have only a limited effect on the along-sound velocity structure.

Interestingly, the depth-averaged subtidal fluctuations were relatively small ($\sim$2–3 cm s$^{-1}$) and uncorrelated between mooring sites suggesting the vertically uniform current response associated with remote wind forcing is of limited importance in Broad Sound. On the other hand, the depth-dependent velocity fluctuations at the subtidal time scale were, in large part ($\sim$36–72%), driven by wind forcing. As indicated by the net flux ratio (mean value of $\sim$0.44), the structure of the local wind response favored vertically sheared flow with the surface currents being direct inward while the bottom currents flowed outward during up-estuary winds (with the reserve occurring during down-estuary winds). This local wind response was associated with the large-scale orientation of Casco Bay rather than the orientation of Broad Sound, which is likely a consequence of the relatively short length-scale of the subsystem. Additionally, during a relative short period ($\sim$3.5 weeks) of current measurements in the deepest point in the bathymetric cross section, the deep channel had fluctuations that were positively correlated with the wind. This unexpected three-layer response to wind forcing is speculated to result from alterations in the density gradient that could arise from the downwelling (or upwelling) of freshwater (denser) water at the head of the bay. Thus, the short, deep nature of Broad Sound appears to be linked to several features associated with the wind-driven circulation.

This study provided new insight into the flow and hydrographic characteristics (e.g., influence of bathymetry on tidal flows, importance and structure of the response to wind forcing at the subtidal frequency, mechanisms associated mean circulation) of a subregion in a weakly stratified, multichannel estuarine/bay system. There was notable spatial and temporal variability in the structure of the along-sound flow field and these findings verified the existence of a laterally sheared flow structure in the mean circulation of Broad Sound, which has important implications on material exchange between inner and outer Casco Bay. More importantly, this study demonstrates the need for improved understanding of the dynamics driving circulation in bathymetrically complex regions with a particular focus on spatial variability in the flow field.

**Acknowledgments**

This experiment was operated by the Physical Oceanography Group (PhOG) at the University of Maine including Patrick Fikes, Neil Fisher, Bob Fleming, Linda Mangum, Mark Neary, Robert Stessel, and John Wallinga. We would also like to thank Rich Pawlowicz at the University of British Columbia for the freely available MATLAB *m_map* toolbox. We are also grateful for the comments by two anonymous reviewers. This work was supported by the NOAA Sea Grant grant R-12-02 and Casco Bay Estuary Partnership (EPA grant 96127201 and EPA grant 96141301). Data used in this study are available at ftp://gyre.umeoce.maine.edu/pub/brian/.

## References

Basdurak, N. B., and A. *Valle*-Levinson (2013), Tidal variability of lateral advection in a coastal plain estuary, *Cont. Shelf Res.*, *61–62*, 85–97, doi:10.1016/j.csr.2013.04.026.

Becherer, J., H. Burchard, G. Flöser, V. Mohrholz, and L. Umlauf (2011), Evidence of tidal straining in well-mixed channel flow from micro-structure observations, *Geophys. Res. Lett.*, *38*, L17611, doi:10.1029/2011GL0490005.

Burchard, H., and R. D. Hetland (2010), Quantifying the contribution of tidal straining and gravitational circulation to residual circulation in periodically stratified tidal estuaries, *J. Phys. Oceanogr.*, *40*, 1243–1262.

Burchard, H., R. D. Hetland, E. Schulz, and H. M. Schuttelaars (2011), Drivers of residual estuarine circulation in tidally energetic estuaries: Straight and irrotational channels with a parabolic cross section, *J. Phys. Oceanogr.*, *41*, 448–570, doi:10.1175/2010JPO4453.1.

Chawla, A., D. A. Jay, A. M. Bapista, M. Wilkin, and C. Seaton (2008), Seasonal variability and estuary-shelf interactions in circulation dynamics of a river-dominated estuary, *Estuaries Coasts*, *31*, 269–288, doi:10.1007/s12237-007-9022-7.

Cheng, P., A. Valle-Levinson, and H. E. Swart (2010), Residual current induced by asymmetric tidal mixing in weakly stratified narrow estuaries, *J. Phys. Oceanogr.*, *40*, 2135–2147.

Cheng, P., A. Valle-Levinson, and H. E. Swart (2011), A numerical study of residual circulation induced by asymmetric tidal mixing in tidally dominated estuaries, *J. Geophys. Res.*, *116*, C01017, doi:10.1029/2010JC006137.

Codiga, D. L., and D. A. Aurin (2007), Residual circulation in eastern Long Island Sound: Observed transverse-vertical structure and exchange transport, *Cont. Shelf Res.*, *27*, 103–116, doi:10.1016/j.csr.2006.09.001.

Emery, W. J., and R. E. Thomson (2004), *Data Analysis Methods in Physical Oceanography*, revised 2nd ed., pp. 379–380, Elsevier, Amsterdam, Netherlands.

Garvine, R. W. (1995), A dynamical system for classifying buoyant coastal discharges, *Cont. Shelf Res.*, *15*, 1585–1596.

Geyer, W. R., and P. MacCready (2014), The estuarine circulation, *Annu. Rev. Fluid Mech.*, *46*, 175–197, doi:10.1146/annurev-fluid-010313–141302.

Hodgkins, G. (1999), Estimating the magnitude of peak flows for streams in Maine for selected recurrence intervals, *U.S. Geol. Surv. Water Resour. Invest. Rep.* 99–4008, U.S. Dep. of the Inter., Augusta, Maine.

Huijts, K. M. H., H. M. Schuttelaars, H. E. de Swart, and A. Valle-Levinson (2006), Lateral entrapment of sediment in tidal estuaries: An idealized model study, *J. Geophys. Res.*, *111*, C12016, doi:10.1029/2006JC003615.

Huijts, K. M. H., H. M. Schuttelaars, H. E. de Swart, and C. T. Friedrichs (2009), Analytical study of the transverse distribution of along-channel and transverse residual flows in tidal estuaries, *Cont. Shelf Res.*, *29*, 89–100, doi:10.1016/j.csr.2007.09.0007.

Janzen, C. D., J. H. Churchill, and N. R. Pettigrew (2005), Observations of exchange between eastern Casco Bay and the western Gulf of Maine, *Deep Sea Res., Part II*, *52*, 2411–2429.

Kasai, A., A. E. Hill, T. Fujiwara, and J. H. Simpson (2000), Effect of the Earth's rotation on the circulation in regions of freshwater influence, *J. Geophys. Res.*, *105*, 16,961–16,969.

Kim, C.-K., and K. Park (2012), A modeling study of water and salt exchange for a micro-tidal, stratified northern Gulf of Mexico estuary, *J. Mar. Syst.*, 96–97, 103–115, doi:10.1016/j.jmarsys.2012.02.008.

Kistner, D. A., and N. R. Pettigrew (1999), Reverse estuarine circulation in the New Meadows Estuary, Maine, American Spring Meeting, Boston, MA, *Eos Trans. AGU*, *79*(1), OS61.

Large, W. G., and S. Pond (1981), Open ocean momentum flux measurements in moderate to strong winds, *J. Phys. Oceanogr.*, *11*, 324–336.

Lee, J., B. M. Webb, B. Dzwonkowski, K. Park, and A. Valle-Levinson (2013), Bathymetric influences on tidal currents at the entrance to a highly stratified, shallow estuary, *Cont. Shelf Res.*, *58*, 1–11. doi:10.1016/j.csr.2013.03.002.

Lentz, S. J. (2008), Observations and a model of the mean circulation over the Middle Atlantic Bight continental shelf, *J. Phys. Oceanogr.*, *38*, 1203–1221, doi:10.1175/2007JPO3768.1.

Lerczak, J. A., and W. R. Geyer (2004), Modeling the lateral circulation in straight, stratified estuaries, *J. Phys. Oceanogr.*, *34*, 1410–1427.

National Ocean Service, 2000. *Tide and Current Glossary*. NOAA, Silver Spring, MD.

Pawlowicz, R., R. Beardsley, and S. Lentz (2002), Classical tidal harmonic analysis including error estimates in MATLAB using T_TIDE, *Comput. Geosci.*, *28*, 929–937.

Scully, M. E., and C. T. Friedrichs (2007), The importance of tidal and lateral asymmetries in stratification to residual circulation in partially mixed estuaries, *J. Phys. Oceanogr.*, *37*, 1496–1511.

Scully, M. E., and W. R. Geyer (2012), The role of advection, straining, and mixing on the tidal variability of estuarine stratification, *J. Phys. Oceanogr.*, *42*, 855–868, doi:10.1175/JPO-D-10–05010.1.

Shearman, R. K., and S. J. Lentz (2003), Dynamics of mean and subtidal flow on the New England shelf, *J. Geophys. Res.*, *108*(C8), 3281, doi:10.1029/2002JC001417.

Signell, R. P., and W. R. Geyer (1991), Transient eddy formation around headlands, *J. Geophys. Res.*, *96*, 2561–2575.

Simpson, J. H., J. Brown, J. Matthews, and G. Allen (1990), Tidal straining, density currents, and stirring in the control of estuarine stratification, *Estuaries*, *13*(2), 125–132.

Sinnett, G. H. (2012), Circulation and transport in Casco Bay, Maine, Master's thesis, electronic theses and dissertations paper 1786, Univ. of Maine, Orono, Maine.

Valle-Levinson, A. (2008), Density-driven exchange flow in terms of the Kelvin and Ekman numbers, *113*, *C04001*, doi:10.1029/2007JC004144.

Valle-Levinson, A. (2011), 2.07 Large estuaries (effects of rotation), in *Treatise on Estuarine and Coastal Science*, edited by E. Wolanski and D. McLusky, pp. 123–140, Academic Press, Waltham, Mass.

Whitney, M. M., and D. L. Codiga (2011), Response of a large stratified estuary to wind events: Observations, simulations, and theory for Long Island Sound, *J. Phys. Oceanogr.*, *41*, 1308–1327, doi:10.1175/2011JPO4552.1.

Wong, K. C. (1994), On the nature of transverse variability in a coastal plain estuary, *J. Geophys. Res.*, *99*, 14,209–14,222.

Wong, K. C., and J. E. Moses-Hall (1998), The tidal and subtidal variations in the transverse salinity and current distributions across a coastal plain estuary, *J. Mar. Res.*, *56*, 489–517.

Xue, H., and Y. Du (2010), Implementation of a wetting-and-drying model in simulating the Kennebec-Androscoggin plume and the circulation in Casco Bay, *Ocean Dyn.*, *60*, 341–357, doi:10.1007/s10236-010-0269-3.

Xue, H., Y. Xu, D. Brooks, N. R. Pettigrew, and J. Wallinga (2000), Modeling the circulation in Penobscot Bay, Maine, edited by L. Spauldng and H. L. Bulter, *Proceedings of the 6th International Conference on Estuarine and Coastal Modeling*, pp. 1112–1127, Am. Soc. of Civ. Eng., Reston, Va.